Design of a Modular Multilevel Converter with 400 kWh of Integrated Batteries

1st Niklas Katzenburg
Elektrotechnisches Institut (ETI)
Karlsruhe Institute of Technology (KIT)
Karlsruhe, Germany
niklas.katzenburg@kit.edu

2nd Kai Kuhlmann
Aschaffenburg UAS
Aschaffenburg, Germany
kai.kuhlmann@th-ab.de

3rd Lars Leister
Elektrotechnisches Institut (ETI)
Karlsruhe Institute of Technology (KIT)
Karlsruhe, Germany
lars.leister@kit.edu

4th Lukas Stefanski
Elektrotechnisches Institut (ETI)
Karlsruhe Institute of Technology (KIT)
Karlsruhe, Germany
lukas.stefanski@kit.edu

5th Johannes Teigelkötter
Aschaffenburg UAS
Aschaffenburg, Germany
johannes.teigelkoetter@th-ab.de

6th Marc Hiller
Elektrotechnisches Institut (ETI)
Karlsruhe Institute of Technology (KIT)
Karlsruhe, Germany
marc.hiller@kit.edu

***Abstract*—In this paper the electromechanical design and the cascaded signal processing platform of a modular multilevel converter with integrated, second-life battery modules are presented. With its 120 full-bridge submodules, the prototype is designed for a maximum in- and output power of $100\,\mathrm{kW}$ and to store up to $400\,\mathrm{kWh}$.**

***Index Terms*—Modular Multilevel Converters (MMC), Energy Storage, Modular Reconfigurable Batteries, Hardware Design**

I. Introduction

The increasing amount of renewable energy sources in the supply grid results in a converter dominated grid and a demand for dynamic energy storage systems with high output voltage quality [1]. A modular multilevel converter (MMC) with integrated lithium-ion batteries satisfies these requirements, since the MMC inherently achieves high output voltage quality [2] and batteries respond more dynamically than other storage devices like fuel cells or flow batteries.

With the rising number of electric vehicles, several megawatt hours of second-life batteries will be available in a couple of years. These batteries typically still have 80 percent of their original capacity, which is deemed unacceptable for electric vehicle operation, but is sufficient for the use in stationary storage applications. In addition to being economically attractive for the owner of the storage system, this use case distributes the ecological costs related to the production of the battery over a longer lifespan, thus reducing the impact of the production on the overall ecological footprint.

Second-life batteries from different manufacturers and of different kinds cannot be simply combined to one big storage system but require additional hardware to operate. Furthermore, a sophisticated energy management can maximize the lifetime of the second-life batteries. Due to its modularity and its degrees-of-freedom regarding the internal energy distribution, an MMC inherently includes an energy management system and is a suitable choice for connecting (second-life) batteries to the supply grid.

With several degrees-of-freedom and a high number of MMC cells, the system complexity and the control effort are significant. To investigate the system behavior and the algorithms to optimize the lifetime of different battery modules integrated in one MMC, a full-scale prototype with a peak power of $100\,\mathrm{kW}$ and a storage capability of $400\,\mathrm{kWh}$ based on real-world, second-life batteries is designed.

Before going into details about the design of the prototype, the MMC in general is briefly introduced and an overview of existing prototypes of MMCs with integrated batteries is given in section II. The most important system parameters of the designed prototype are derived in section III. They are then incorporated in the electromechanical design and the concept of the signal processing platform in section IV. To conclude, exemplary measurements of the power electronic module (PEM) and one arm of the MMC are presented in section V.

II. Modular multilevel converter

The MMC is a modular converter consisting of several identical PEMs, also called MMC cells or submodules, and was introduced in [2]. These PEMs typically consist of a half or full bridge fed by a capacitor without any additional, isolated power supply. Several PEMs and an inductor are connected in series to make one arm of the MMC. Two arms are then combined to form one phase as seen in Fig. 1. The phases are connected in parallel with each other and the DC side.

MMCs are commonly used for high voltage DC transmission (HVDC) or medium voltage drive applications. Recently they have gained interest as energy storage systems with integrated power electronics for low and medium voltage applications due to the growing demand of energy storage systems for grid applications and electric vehicles [3]–[9]. For this kind of usage the energy storage capability of each PEM is extended by adding a battery or - generally speaking - an

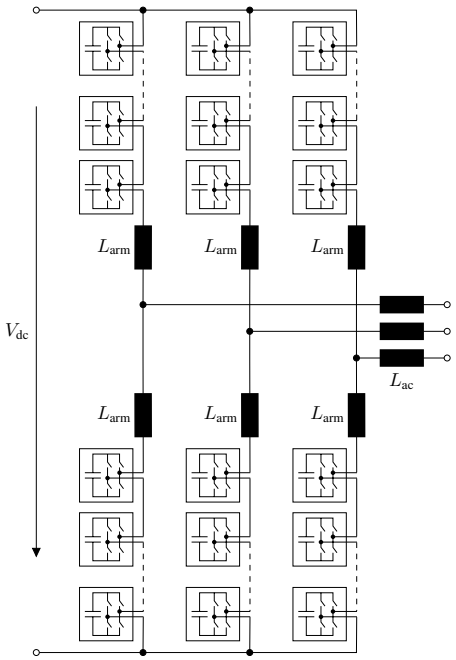

Fig. 1: Equivalent circuit of an MMC.

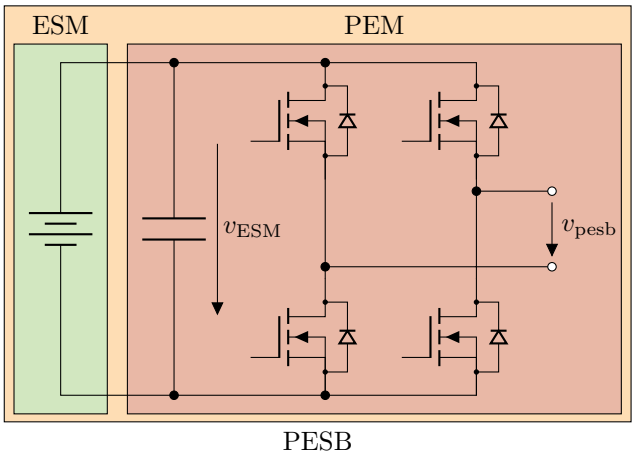

Fig. 2: Equivalent circuit of one PESB.

energy storage module (ESM) in parallel to the capacitor as seen in Fig. 2. For this configuration, the term power electronic storage block (PESB) was introduced in [10], and is also used in this paper.

MMCs with such PESBs offer the same advantages as conventional MMCs like high output voltage quality, high modularity and easy scalability [2]. In addition, integrating batteries in the individual PEMs instead of connecting one high voltage battery to the DC side of the MMC allows to easily combine different battery types in one energy storage system and to operate these in a lifetime optimizing way. This is especially interesting for second-life batteries from electric vehicles or home storage applications.

A. MMC with integrated batteries

One of the earliest publications suggesting to integrate batteries into an MMC is [4]. There, a system with six PESBs per arm with a nominal voltage of $v_{\text{ESM}} = 600\,\text{V}$ each is simulated. Its rated power in the simulation is $5\,\text{MW}$.The DC side has $6\,\text{kV}$, the AC side is connected to a grid with a Root Mean Square (RMS) phase voltage of $2.4\,\text{kV}$. Simulations for three different modes of operation - power transfer from DC to AC, batteries to AC and batteries to DC and AC - are presented to demonstrate the functionality of the converter. However, no prototype is presented.

Since this work focuses on the design of a full scale prototype for grid applications, the next paragraphs only focus on publications about MMCs with integrated batteries, where a prototype was built. A chronologically sorted overview of these is given in Table I.

The prototypes in [11] and [12] both employ PEMs based on a half-bridge with an additional DC/DC converter to decouple the battery voltage from the input voltage of the half-bridge. The prototypes are mainly used to demonstrate the general functionality of the system and to validate simulation results. It should be noted, that the prototype in [11] only includes battery modules in one phase of the three-phase prototype.

The same topology of the PEM is used in [13], [14] for a three-phase prototype to validate state of health testing and equalization methods. Each battery module is additionally equipped with a custom battery management system (BMS).

In contrast to the previously mentioned prototypes, the ones presented in [8], [15]–[19] directly connect the battery to the half-bridge of the PEM. This way, the output voltage of the PEM is directly determined by the voltage of the ESM, but two switches and one inductance can be saved and the control effort is reduced. The prototype in [18], [19] slightly differs from the other ones listed, since the PESBs in the lower arm of the single-phase prototype include capacitors with $4.7\,\text{mF}$ as ESMs instead of battery modules. The respective MMC is controlled in such a way, that the capacitors buffer power fluctuations with high frequencies, whereas the batteries store energy for the long term demand.

The MMC is not the only topology used for energy storage systems with integrated power electronics, but other topologies, including the star- or delta-connected cascaded H-bridge converter [3], [20], [21], the modular multilevel series parallel converter (MMSPC) [22], [23] and the so called battery modular multilevel management (BM3) converter [24], are also employed. Prototypes are presented in [3], [20], [23], [24]. Since all of these topologies make it more complicated to include a DC side, which is desired for the presented system, they are not discussed in more detail.

III. System Parameters

The presented prototype is conceived as an energy storage system for an existing industrial micro grid. With the DC side of the MMC, renewable energies with fluctuating availability can be easily integrated. For example, the plot in Fig. 3 compares the available power of a photovoltaic plant at an

TABLE I: Parameters of existing prototypes of MMCs with integrated batteries

Publication	Output power in kW	Output voltage in V	Number of PESB per arm	Topology of PEM	Nominal voltage of ESM in V	Technology of ESM	Stored energy in kWh
[11]	25	187.5	4	HB w/ DC/DC	52[a]	lithium-ion	12.5[a]
[12][b]	4	113[a]	4	HB w/ DC/DC	25.6	LiFePO4	0.6
[8], [15]–[17]	0.06	17.5	2	HB	36	lead-acid	1.43
[13]	not given	220	7	HB w/ DC/DC	54	lithium-ion	5.67
[14]	2.4	220	12	HB w/ DC/DC	54	lithium-ion	9.59
[18], [19][b]	not given	40	3	HB	48	lead-acid	1

[a]Estimated value. [b]Single-phase prototype.

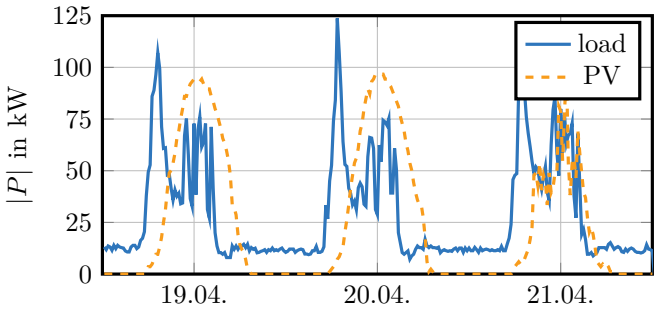

Fig. 3: Exemplary load profile of an industrial micro grid.

industrial micro grid with the power demand of the same. It can be clearly seen that the main peak in the power demand from the cafeteria does not coincide with the maximum available power from the PV plant. The excess power from the PV plant could be stored in the presented MMC and be used to mitigate the differences in offered and demanded power during night time.

For the specific use case depicted in Fig. 3, a peak in- and output power of 100 kW is desired to handle the full power from the PV plant. The excess demand from the load will be fed from the grid, while the MMC is used to shave these load peaks. This results in an RMS current I_{ac} = 144 A per phase, since the AC side is connected to the low voltage grid with a RMS voltage of 230 V per phase. Assuming a symmetrical operation of the MMC, this yields an RMS current I_{arm} = 72 A per arm. To allow for balancing currents, a margin of approximately 10 % is added. Thus, for the dimensioning of the PEMs, the arm inductors and the other components a maximum RMS arm current $I_{\mathrm{arm,max}} = 80\,\mathrm{A}$ is assumed.

The arm inductors are designed to limit the peak-to-peak value of the ripple current in each arm to the allowable maximum $\Delta i_{\mathrm{arm,pp,max}} = 8\,\mathrm{A}$, which is chosen as 10 % of the maximum RMS arm current. The required inductance can be determined according to

$$L_{\mathrm{arm,min}} = \frac{v_{\mathrm{PESB,max}}}{f_{\mathrm{sw,eff}} \cdot \Delta i_{\mathrm{arm,pp,max}}}\,, \tag{1}$$

with the maximum voltage step $v_{\mathrm{PESB,max}} = 58.1\,\mathrm{V}$ and the effective switching frequency $f_{\mathrm{sw,eff}}$. The latter is determined through the individual switching frequency of the PEMs $f_{\mathrm{sw,PEM}}$ and the number of PESBs switched during one control period $T_{\mathrm{C}} = 125\,\mu\mathrm{s}$. Each half-bridge is switched with the control frequency $f_{\mathrm{C}} = 8\,\mathrm{kHz}$. Since the switching events of the two half-bridges on one PEM are alternated, an output frequency of $f_{\mathrm{sw,PEM}} = 16\,\mathrm{kHz}$ results. With all 20 PESBs being switched once during one control period, the effective switching frequency is 320 kHz and (1) yields a minimum inductance of 93.8 µH. The actual inductance is chosen to 100 µH.

IV. System Design

Based on the desired parameters from section III, the following sections describe the electromechanical design and the conceived signal processing platform of the prototype.

A. Power electronic storage block

As depicted in Fig. 2 each PESB consists of an ESM, respectively a battery module in this paper, and the PEM. Second-life battery modules with a nominal voltage of $U_{\mathrm{BM,n}} = 51.1\,\mathrm{V}$ and a nominal capacity of $Q_{\mathrm{BM,n}} = 66\,\mathrm{Ah}$ from home storage applications are used. They will be combined with new batteries of the same making. Other types of battery modules could also be included, if their maximum voltage does not exceed 70 V due to the used MOSFETs. Nonetheless, the concept of this prototype and the cascaded signal processing platform could also be applied to modules from second-life batteries from electric vehicles.

With the nominal voltage of $U_{\mathrm{BM,n}} = 51.1\,\mathrm{V}$ and the desired arm voltage of 700 V, at least 14 battery modules - which corresponds to the number of MMC cells - per arm are required. To allow for more flexibility in the control strategy - especially at low voltages, respectively a low state of charge (SoC), of the battery modules - $N = 20$ cells per arm are chosen resulting in 120 battery modules in total. This also reduces the load on the individual battery modules to stay within their allowed limits of a continuous current of 30 A and a peak current of 40 A, respectively. Still, for the desired output power of 100 kW it would be beneficial to replace some of the second-life battery modules with high power ones. With the given battery modules, the total energy stored in the MMC,

$$E_{\mathrm{MMC}} = N \cdot U_{\mathrm{BM,n}} \cdot Q_{\mathrm{BM,n}} \approx 404.7\,\mathrm{kWh}\,, \tag{2}$$

at the nominal voltage of the battery modules is calculated.

The PEMs are split into the actual power unit and the local control unit (LCU), which is described in subsection IV-B. To

achieve more flexibility in controlling the energy flow of the batteries, i.e., to decouple the direction of the current through the ESM i_{ESM} and the current of the respective arm i_{arm}, a full-bridge topology is chosen. This also allows a varying voltage at the DC side of the MMC.

To enable operation of the PEM in case no battery module is connected, the capacitance C_{ESM} in the DC link is added. Its size is determined by the maximum allowable pulsation of the voltage of the capacitors

$$\Delta V_{\mathrm{C_{ESM}}} = V_{\mathrm{C_{ESM},max}} - V_{\mathrm{C_{ESM},min}}\,, \tag{3}$$

where $V_{\mathrm{C_{ESM},max}} = 70\,\mathrm{V}$ and $V_{\mathrm{C_{ESM},min}} = 35\,\mathrm{V}$ are the maximum and the minimum voltage of the capacitor. This directly relates to the maximum energy pulsation

$$\Delta E_{\mathrm{C_{ESM}}} = \frac{1}{2}\cdot C_{\mathrm{ESM}}\cdot\left(V^2_{\mathrm{C_{ESM},max}} - V^2_{\mathrm{C_{ESM},min}}\right) \tag{4}$$

of the capacitor when no battery module is connected. The occurring energy ripple without any compensation through control algorithms is determined as

$$\Delta E_{\mathrm{C_{ESM}}} = \frac{\hat{I}_{\mathrm{ac}}}{\omega_{\mathrm{ac}}}\cdot\frac{V_{\mathrm{dc}}}{2\cdot N}\cdot\left[1-\left(\frac{\hat{V}_{\mathrm{ac}}\cdot\cos(\varphi_{\mathrm{ac}})}{V_{\mathrm{dc}}}\right)^2\right]^{\frac{3}{2}} \tag{5}$$

according to [2], [25]. With the current amplitude $\hat{I}_{\mathrm{ac}} \approx 205\,\mathrm{A}$, the frequency of the AC grid $\omega_{\mathrm{ac}} = 50\,\mathrm{Hz}$, the DC voltage $V_{\mathrm{dc}} = 700\,\mathrm{V}$, the amplitude of the AC grid voltage $\hat{V}_{\mathrm{ac}} \approx 325\,\mathrm{V}$ and the worst case power factor $\cos(\varphi_{\mathrm{ac}}) = 0$, equations (4) and (5) can be combined and rearranged to obtain a minimum capacitance of $C_{\mathrm{ESM,min}} = 6.2\,\mathrm{mF}$. The actual capacitance is chosen to $C_{\mathrm{ESM}} = 6.8\,\mathrm{mF}$.

Due to the maximum voltage of the battery modules of about 60 V, the IPTC015N10NM5 MOSFETs from Infineon rated for 100 V are chosen as semiconductors. These MOSFETs are in the novel TO-Leaded top-side cooling (TOLT) package to achieve better heat dissipation from the semiconductors to the heatsinks above [26]. The TOLT package has an additional drain pad on the top side to easily mount a heat sink and minimize the thermal resistance $R_{\mathrm{th,j-amb}}$ between the junction and the surrounding air. To further reduce the heat dissipation by minimizing the losses, three MOSFETs are connected in parallel per switch. Each half-bridge is covered by a finned heat sink with an electrically insulating thermal gap pad in between to minimize the thermal resistance. These heat sinks are not mounted on the prototype of the PEM shown in Fig. 4, because they would obstruct the view on the semiconductors.

B. Electromechanical design

The 120 battery modules take up about $2.2\,\mathrm{m}^3$ and weight $2.6\,\mathrm{t}$ in total. Therefore, the main concern for the electromechanical system design is how to package the battery modules in such a way that the following requirements are met.

Due to the use as a research prototype, the components of the MMC need to be well accessible to allow for easy maintenance and reconfiguration of the setup while maintaining mechanical integrity. To ensure the latter and split the battery modules into reasonable sized cabinets in terms of volume and weight, they are divided into six groups, inherently given by the six arms of an MMC. With this segmentation, it is desirable to design each cabinet in such a way, that each arm can be put into operation independently.

In each cabinet, the battery modules are split into five groups of four modules per floor of the cabinet as shown in Fig. 5. Since the potential of each PESB is floating and varies based on the current operating point, all PESBs are isolated from the cabinet with its potential on protective ground with a panel made of polycarbonate (PC).

This configuration introduces a parasitic capacitance

$$C_{\mathrm{BM,par}} = \epsilon_0\cdot\epsilon_{\mathrm{PC}}\cdot\frac{A_{\mathrm{BM}}}{d_{\mathrm{PC}}} \tag{6}$$

into the system, which must be sufficiently low to avoid leakage currents. Since the battery modules are placed on their side, the effective area approximates to $A_{\mathrm{BM}} = 546.1\,\mathrm{mm}\cdot 216.8\,\mathrm{mm} = 118.4\times10^{-3}\,\mathrm{m}^2$. A relative permittivity of PC of $\epsilon_{\mathrm{PC}} = 3$ is assumed. With a thickness of $d_{\mathrm{PC}} = 6\,\mathrm{mm}$, the resulting parasitic capacitance per battery module is $C_{\mathrm{BM,par}} = 550\,\mathrm{pF}$. Inserting this and the maximum voltage transient of $3.2\,\mathrm{kV\,\mu s^{-1}}$ during a switching event of the MOSFETs into

$$i_{\mathrm{leak}} = C_{\mathrm{BM,par}}\cdot\frac{\mathrm{d}V}{\mathrm{d}t}\,, \tag{7}$$

yields a peak leakage current of $i_{\mathrm{leak}} = 1.6\,\mathrm{A}$ per battery module. However, this peak only occurs for less than $10\,\mathrm{ns}$ during the transient switching event and is therefore deemed acceptable.

In addition to the PESBs and the arm inductance, each cabinet includes a 19"-rack in between the third and the fourth floor as seen in Fig. 5. The local signal processing platform, the Arm Control Unit (ACU), two contactors to disconnect the cabinet, the measurement of the arm current and the pre-charge circuitry are located in this rack.

To connect all six arms to each other and to the laboratory test infrastructure, a seventh, smaller cabinet is used. The connections to the DC and the AC side are both individually fused and can be decoupled in case of a failure with dedicated

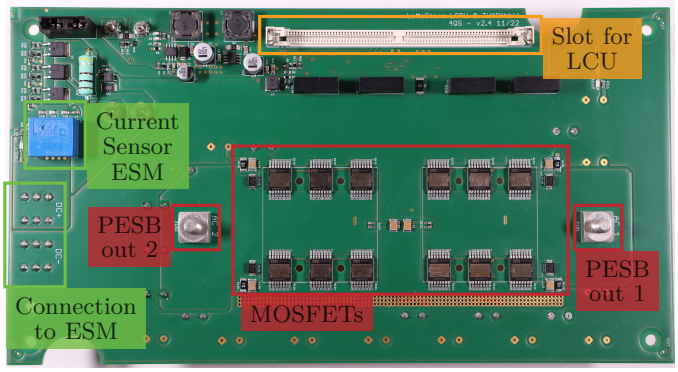

Fig. 4: Prototype PCB of the power electronic module.

contactors. Additionally, the central signal processing platform to control the voltages and currents on the DC and the AC side as well as the computer to monitor the prototype and the laboratory infrastructure are located here.

C. Signal processing platform

Analogous to the electromechanical design, the signal processing of the MMC is divided in the cascaded structure depicted in Fig. 6. The top level control of the MMC and the energy management system are implemented on the central control unit (CCU) which is based on a *Zynq 7030* System-on-Chip with two ARM cores and one Field Programmable Gate Array (FPGA). The System-on-Chip is placed on a carrier offering eight slots for expansion cards implementing the fiber optic communication (FOC) between the different cabinets, interfaces for the measurement of voltages and currents and general purpose input/output (GPIO) functionality. More details about the in-house developed hardware and the rapid control prototyping workflow of the CCU can be found in [27].

On the CCU the overall control of the MMC and the energy management for the battery modules including the lifetime optimization, which sets the desired operating point for all 120 battery modules [10], are implemented. The overall control of the MMC mainly consists of the controllers for the voltages and currents on the AC and the DC side as well as the energy balancing between the arms of the MMC resulting in the reference voltages for the arms $\underline{v}_{\mathrm{arm,ref}}$ [28]. The reference voltages for all six arms and the desired operating points of all 120 battery modules are transferred to the arms via FOC and processed by a dedicated control platform, the ACU, in each arm.

The ACU is based on a *MAX10* FPGA with 50 000 logic elements, which is placed on a carrier board offering slots for interface cards. Its main functionalities are the handling of the communication between the PESBs, and the CCU as well as the calculation of the reference voltages for the PEMs with $v_{\mathrm{arm,ref}} = \sum_{i=1}^{20} v_{\mathrm{PESB,ref},i}$. Additionally, the analog-to-digital conversion (ADC) of the measurement of the arm current and a state machine for functional safety are implemented on the ACU.

The LCU relies on the TMS320F280023 real-time microcontroller with various onboard modules, e.g., CAN, UART, ADC, PWM, to implement the required functionality, like the communication with the battery module and the ACU. The software is based on the so-called rate-monotonic scheduling, where all tasks are called in order according to their priority, to fulfill the real-time requirement. In the highest priority task, the recording of all measured values like the voltage of the capacitor and the battery current, the communication with the ACU and the control of the semiconductors are handled. In addition, two slow communication tasks are implemented to grab all necessary data from the CAN of the BMS integrated in the battery modules.

The conceived architecture of the signal processing defines a clear separation between the top level control in combination with the energy management in the CCU, the control of each arm in the corresponding ACU and the low level control of the PEMs by the respective LCUs. This approach improves the modularity and the scalability of the prototype, which is beneficial for putting the system into operation and extending it with more PESBs in the future.

D. Communication protocol

The communication protocols for both, the communication between the CCU and the ACUs and the communication between the ACUs and the LCUs respectively, are based on the UART protocol transmitted via FOC.

On top of both protocols another layer is implemented to decode the sent words into actual data, e.g., reference values or measured values, and to allow for different data to be sent in different cycles. This is used to retrieve all data from the individual battery modules, e.g., temperatures, cell voltages and SoC, without overloading the communication. Therefore, different frames distinguished by unique IDs are introduced.

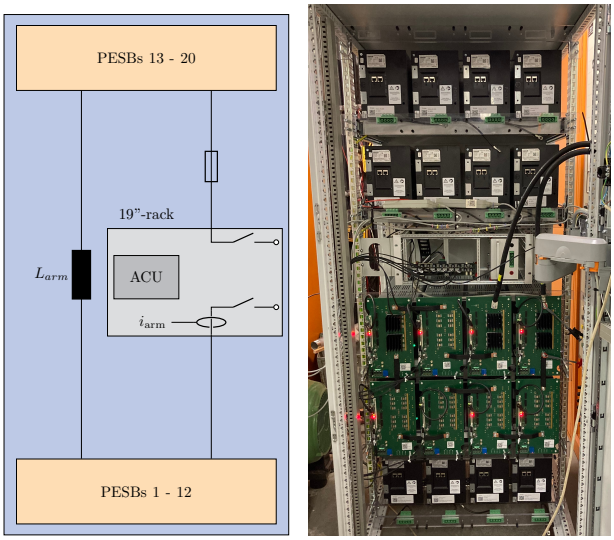

(a) Schematic (b) Prototype.

Fig. 5: Cabinet of an arm.

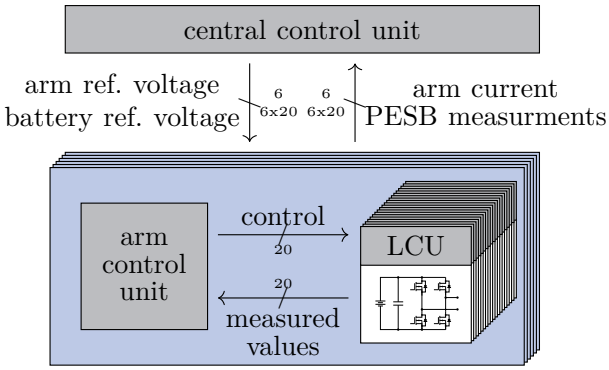

Fig. 6: Cascaded control structure.

The frame to be transmitted in the next control period is always requested by the higher control structure, i.e., the CCU requests frames from the ACUs and each ACU requests frames from the PESBs.

In addition to the different frames, the protocol between CCU and ACUs allows for cyclic data. This is used to transmit information about the PESBs which is split in critical information, i.e., the voltage and the current of each battery module, and in less critical information like the SoC or the temperature of the battery. The critical information for one PESB is updated with a frequency of $400\,\mathrm{Hz}$ in the CCU and the other information with $50\,\mathrm{Hz}$. In the ACU, the information is updated with the control frequency $f_\mathrm{C} = 8\,\mathrm{kHz}$ and averaged between two transmissions to the CCU. The measured arm current and the status from the ACU are also updated with f_C in the CCU.

The update rate of the data from the ESM in the CCU is sufficiently high, since each ESM contains a dedicated BMS including features to protect against undervoltage, overvoltage, -current and -temperature. The information collected by the BMS are only updated with a frequency between $0.33\,\mathrm{Hz}$ and $2\,\mathrm{Hz}$ depending on the kind of data. Additionally, the energy management, which has not been tested with the prototype yet, will run with a low update frequency of $20\,\mathrm{Hz}$.

V. Prototype Measurements

To test the basic functionality of the PEM and the cascaded control structure, exemplary measurements are conducted. First, the developed PEM is evaluated in subsection V-A. Afterwards, it is demonstrated that the combination of several PEM can be operated with the cascaded control structure in subsection V-B.

A. Power electronic module

To verify the performance and the thermal behavior of the designed PEM, it is tested under the maximum rated current conditions described in section III. As depicted in Fig. 7, heating up of the PCB, respectively of the heat sink, is limited to about $\Delta T \approx 30\,\mathrm{K}$ above ambient temperature, using only the natural convection of air through the fins. With the input power $P_\mathrm{in} \approx 1670\,\mathrm{W}$ and the measured power dissipation $P_\mathrm{loss} \approx 35\,\mathrm{W}$, the designed PEM achieves an overall efficiency, including the auxiliary power supply for the microcontroller and all peripherals, of about $\eta_\mathrm{PEM} \approx 97.5\,\%...98\,\%$.

B. One arm of the modular multilevel converter

To demonstrate the basic functionality of the prototype, especially the cascaded control structure, exemplary measurements with the already existing part of one of the six arms are conducted. The test setup consists of eight PESBs connected in series with a R-L load with $120\,\Omega$ and $125\,\mu\mathrm{H}$. The arm inductance is not connected. They are controlled by one ACU, which in return is controlled by the CCU. In the tested scenario, the CCU requests a sine with an amplitude of $320\,\mathrm{V}$ and the typical German grid frequency of $50\,\mathrm{Hz}$. The resulting output voltage across the R-L load and the respective current are shown in Fig. 8. All data is measured with oscilloscopes with a sample rate of $1.25\,\mathrm{MSa\,s^{-1}}$.

The switched output voltage of one PEM as well as the current and the voltage of the corresponding battery module are shown in Fig. 9. The sign of the output voltage of the PEM in Fig. 9 (a) corresponds to the sign of the overall output voltage in Fig. 8. The detailed plot in Fig. 9 (b) depicts the switching behavior of the PEM and the respective switching frequency of $16\,\mathrm{kHz}$.

Due to the high energy of the battery module and the short time span, the output voltage of the battery module in Fig. 9 (c) is constant except for the ripple induced by the switching of the PEM. The current through the battery module in Fig. 9 (d) is dominated by the behavior of the overall output current. However, since there is a passive load connected, the current through the battery is only positive - meaning the battery is being discharged - except for the ripple induced by the switching of the PEM and the parallel capacitor, respectively.

VI. Conclusion

In this paper, an overview of existing prototypes of MMCs with integrated batteries is given. Most of these are small scale prototypes and lack the integration of second-life battery modules from real-life applications.

To investigate the usage of a full scale MMC with integrated batteries as an industrial energy storage system, a new prototype is conceived. The primary research objectives are the combination of different kinds of battery modules, e.g.,

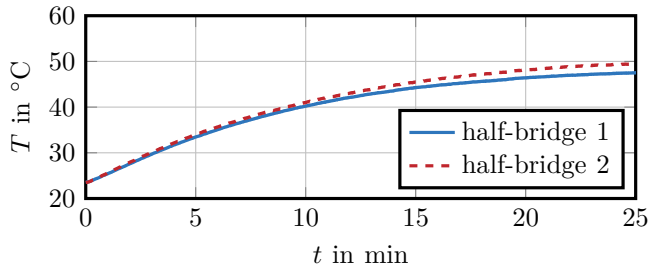

Fig. 7: Temperature rise at maximum current load.

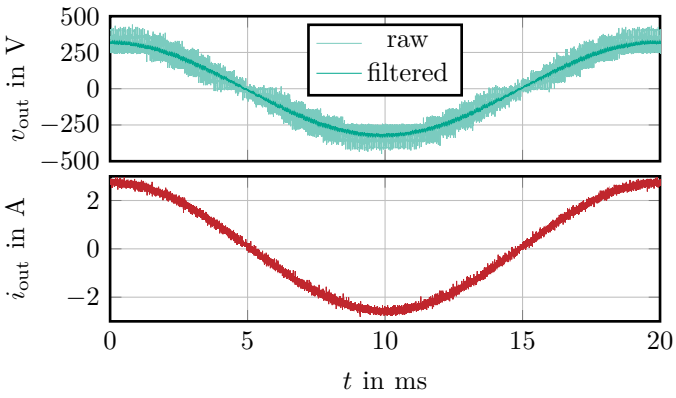

Fig. 8: Output voltage and current.

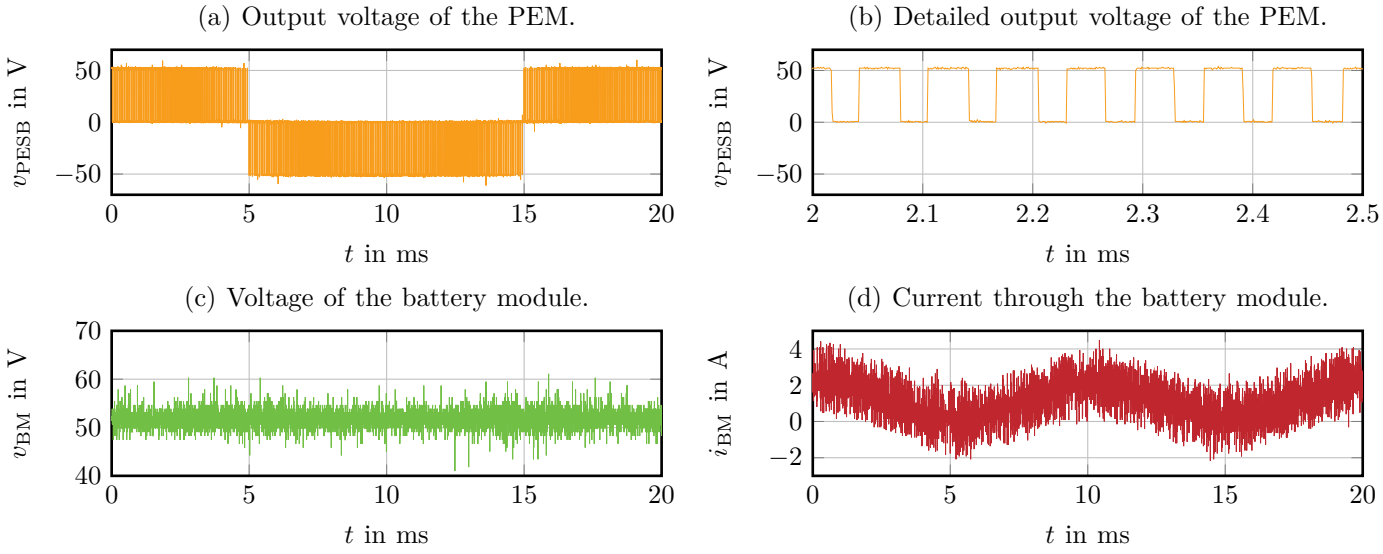

Fig. 9: Measured quantities of one PESB.

used and new (high power) battery modules, and the lifetime optimized operation of these. For the mentioned use case, a maximum power of 100 kW and a storage capability of approximately 400 kWh are targeted.

The challenges arising with a full-scale prototype are analyzed and solutions for the electromechanical design on system- and submodule-level are presented. Additionally, the distributed signal processing platform including the designed communication protocols is laid out.

Measurements conducted with a single PEM proof its performance. The first of six cabinets for the arms of the MMC is currently being build and put into operation. An exemplary measurement demonstrates the functionality of the cascaded control structure and the ability of one arm to deliver the desired voltage. Further work will focus on putting the whole system into operation, designing respective control algorithms and conducting measurements to proof their functionality.

Acknowledgement

The authors acknowledge the financial support by the Federal Ministry for Economic Affairs and Climate Action of Germany in the project LeMoStore (project number 03EI4031A-E). Additionally, the authors would like to thank Mainsite GmbH & Co. KG for providing the exemplary load profile presented in this paper.

References

[1] P. v. Tichelen *et al.*, *Preparatory study on ecodesign and energy labelling of batteries under FWC ENER/C3/2015-619-Lot 1. Task 2*. 2019.

[2] R. Marquardt *et al.*, "Modulares stromrichterkonzept für netzkupplungsanwendungen bei hohen spannungen," 2002.

[3] L. Baruschka *et al.*, "Comparison of cascaded h-bridge and modular multilevel converters for BESS application," in *2011 IEEE Energy Conversion Congress and Exposition*, Phoenix, AZ, USA, 2011.

[4] I. Trintis *et al.*, "A new modular multilevel converter with integrated energy storage," in *IECON 2011*, Melbourne, Vic, Australia, 2011.

[5] M. Schroeder *et al.*, "The idea of a modular multilevel converter with integrated batteries," in *2012 International Conference on Smart Grid Technology, Economics and Policies (SG-TEP)*, Nuremberg, Germany, 2012.

[6] A. Hillers *et al.*, "Optimal design of the modular multilevel converter for an energy storage system based on split batteries," in *EPE'13*, Lille, France, 2013.

[7] M. Schroeder *et al.*, "Integration of batteries into a modular multilevel converter," in *EPE'13*, Lille, France, 2013.

[8] F. Gao *et al.*, "State-of-charge balancing control strategy of battery energy storage system based on modular multilevel converter," in *ECCE'14*, Pittsburgh, PA, USA, 2014.

[9] L. Komsiyska *et al.*, "Critical review of intelligent battery systems: Challenges, implementation, and potential for electric vehicles," *Energies*, vol. 14, no. 18, 2021.

[10] L. Leister *et al.*, "Hardware-in-the-loop setup for a modular multilevel converter with integrated batteries," in *2022 IEEE 23rd COMPEL*, Tel Aviv, Israel, 2022.

[11] M. Schroeder *et al.*, "Measurement results of a modular energy storage system unevenly equipped with lithium-ion batteries," in *EPE'15 ECCE-Europe*, Geneva, 2015.

[12] M. Vasiladiotis *et al.*, "Analysis and control of modular multilevel converters with integrated battery energy storage," *IEEE Transactions on Power Electronics*, vol. 30, no. 1, 2015.

[13] Z. Ma *et al.*, "An online SOH testing method of MMC battery energy storage system," in *2018 IEEE 19th COMPEL*, Padua, 2018.
[14] Z. Ma *et al.*, "Multilayer SOH equalization scheme for MMC battery energy storage system," *IEEE Transactions on Power Electronics*, vol. 35, no. 12, 2020.
[15] L. Zhang *et al.*, "Interlinking modular multilevel converter of hybrid AC-DC distribution system with integrated battery energy storage," in *2015 IEEE Energy Conversion Congress and Exposition (ECCE)*, 2015.
[16] Nan Li *et al.*, "Hybrid predictive control method for battery integrated modular multilevel converter," in *2016 IEEE 8th International Power Electronics and Motion Control Conference (IPEMC-ECCE Asia)*, Hefei, China, 2016.
[17] N. Li *et al.*, "SOH balancing control method for the MMC battery energy storage system," *IEEE Transactions on Industrial Electronics*, vol. 65, no. 8, 2018.
[18] L. Zhang *et al.*, "A modular multilevel converter-based grid-tied battery-supercapacitor hybrid energy storage system with decoupled power control," *IPEMC-ECCE Asia*, 2016.
[19] L. Zhang *et al.*, "Decoupled power control for a modular-multilevel-converter-based hybrid AC–DC grid integrated with hybrid energy storage," *IEEE Transactions on Industrial Electronics*, vol. 66, no. 4, 2019.
[20] N. Kawakami *et al.*, "Development of a 500-kW modular multilevel cascade converter for battery energy storage systems," *IEEE Transactions on Industry Applications*, vol. 50, no. 6, 2014.
[21] F. Jauch *et al.*, "Novel isolated cascaded half-bridge converter for battery energy storage systems," in *EPE'14-ECCE Europe*, Lappeenranta, Finland, 2014.
[22] S. M. Goetz *et al.*, "Modular multilevel converter with series and parallel module connectivity: Topology and control," *IEEE Transactions on Power Electronics*, vol. 30, no. 1, 2015.
[23] T. Merz *et al.*, "Optimizing utilization of an MMSPC with model predictive control," in *2020 IEEE 21st COMPEL*, Aalborg, Denmark, 2020.
[24] M. Kuder *et al.*, "Battery modular multilevel management (BM3) converter applied at battery cell level for electric vehicles and energy storages," 2020.
[25] J. Kolb *et al.*, "Dimensioning and design of a modular multilevel converter for drive applications," in *2012 EPE-ECCE Europe*, Novi Sad, Serbia, 2012.
[26] I. T. AG, "Whitepaper - the TOLx family: TOLL, TOLG, TOLT," 2021.
[27] B. Schmitz-Rode *et al.*, "A modular signal processing platform for grid and motor control, HIL and PHIL applications," in *IPEC-Himeji 2022-ECCE Asia*, Himeji, Japan, 2022.
[28] D. Braeckle *et al.*, "Energy pulsation reduction in modular multilevel converters using optimized current trajectories," *IEEE Open Journal of Power Electronics*, vol. 2, 2021.